AUT Journal of Modeling and Simulation

AUT J. Model. Simul., 54(2) (2022) 173-184
DOI: 10.22060/miscj.2023.21110.5271

Modeling of the Earth's rotation variations using a novel approach inspired by the brain emotional learning

A. Hakimi[1], S. A. Monadjemi[1,3], S. Setayeshi[2]*

[1] Department of AI, Faculty of Computer Engineering, University of Isfahan, Isfahan, Iran
[2] Department of Energy Engineering and Physics, Amirkabir University of Technology, Tehran, Iran
[3] School of Continuing and Lifelong Education, National University of Singapore, Singapore

ABSTRACT: DT is a quantity that converts universal time (UT; defined by the Earth's rotation) to terrestrial time (TT; independent of Earth's rotation). The DT values during the time show the Earth's rotation variations. Solar activities and the gravitational force of major solar system components are known as astronomical-based factors that can provide these variations. Recently, several models have been proposed to interpolate and forecast the DT values. Structurally, all mentioned methods have just used past DT values for modeling. In this paper, we propose a novel approach for modeling DT based on the brain's emotional learning with respect to astronomical-origin-based factors effective on the Earth's rotation as the emotional input signals. This model, which employs memory units in the amygdala and orbitofrontal parts, can be named Memory-Based Brain Emotional Learning (MBBEL). MBBEL was run using the data from 1900 to 2000 and 2000 to 2019 as training and testing stages, respectively. After the modeling process, the mean absolute error (MSE) and maximum absolute error (MaxAE) of the train and test stages were 0.011, 0.051, 0.10, and 0.295, respectively. Comparing the MBBEL results against those of eight prior models revealed that MBBEL results considerably improved compared to those of the previous models.

Review History:
Received: Feb. 16, 2022
Revised: Sep. 19, 2022
Accepted: Jan. 14, 2023
Available Online: Feb. 28, 2023

Keywords:
DT
Time series
Brain emotional learning
Amygdala-Orbitofrontal System

1- Introduction

Time measurement in human life is ordinary. Just look at the clock! However, it can be intricate for astronomers. Verily, time scales are based on astronomical phenomena. Two different kinds of time scales have been used in modern astronomy. The first one is based on the Earth's rotation (ER) and typified by Universal Time (UT), and the second one relies on the revolution of Earth in its orbit around the Sun. This concept was implemented in Ephemeris Time (ET) [1].

The rotation of the Earth as the base of UT is somewhat irregular, and several factors can cause this irregularity [2]. These factors can be categorized into geophysical, loading, angular momentum, and gravitational force factors, along with solar activities as a new known factor [3-8]. According to the mentioned studies, geophysical factors include plate tectonics, regional tectonics, Earth's interior, convection, volcanism, and earthquakes. In addition, loading factors are oceans, atmosphere, glaciers, and groundwater. Further, oceanic, atmospheric, and Earth's liquid core are among the angular momentum factors. Finally, gravitational force factors encompass Earth tides, precession, and mutation. However, the type and extent of the effect of these factors on each other and ER are not fully understood yet. In this respect, solar activities and the gravitational force of the sun, the moon, and solar system planets can differ from the others due to their astronomical origin.

As UT is moderately irregular in its rate, astronomers presented ET; it is the independent variable of time in Simon Newcomb's *Tables of the Sun*, which formed the basis of all astronomical ephemerides from 1900 through 1983. In 1984, ET was replaced by Terrestrial Dynamical Time (TDT) as the independent argument for apparent geocentric ephemerides. The unit of TDT is a day of 86400 SI seconds at mean sea level. In 1991, TDT was renamed Terrestrial Time (TT), which is considered to be a uniform time-scale and used as the time logic for the predictions of astronomical events in dynamical theories [9].

Eclipse predictions are computed in TT. To convert TT predictions to UT, we must know the difference between TT and UT. This parameter is known as DT (Delta T, delta-T, deltaT, or ΔT) and can be expressed by Eq. (1) as follows [10]:

$$DT = TT - UT \tag{1}$$

The time series of DT values shows the variations in the ER and the length of the day [9]. These values are estimated by investigating hundreds of eclipse observations (both solar and lunar) before 1600 CE, recorded in early European, Middle Eastern, and Chinese annals, manuscripts, and canons

*Corresponding author's email: setayesh@aut.ac.ir

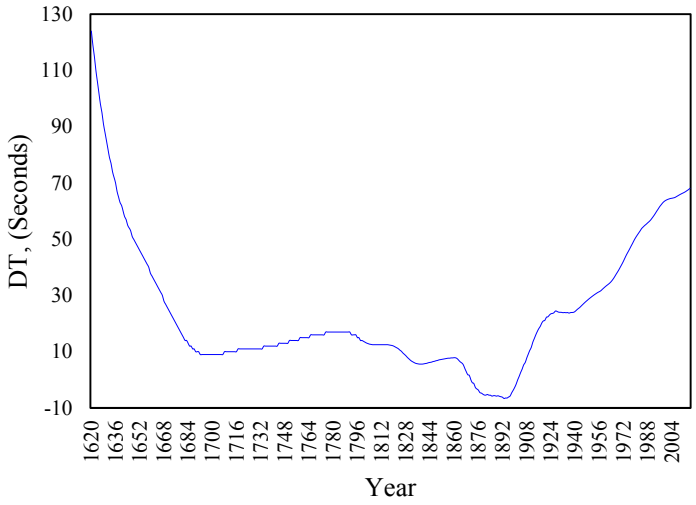

Fig. 1. Time series diagram of DT values (time difference obtained by subtracting universal time from the terrestrial time) from 1620 to 2018

according to previous research [11-17]. Despite their relatively low precision, these data represent the only evidence of the DT value for this period. DT values were reported after using telescopes to observe the lunar occultation of stars. Then, quasars' atomic clocks and radio observations were used to determine these values [3-19]. Therefore, the precise DT values have been available since 1620. Fig. 1 illustrates these values from 1620 to 2018. As shown, the length of the day increases highly gradually. In fact, ER has been slowed over the last century.

As mentioned earlier, DT is applied as a correction parameter in a variety of astronomical calculations and predictions. Thus, modeling and forecasting this parameter are important for astronomers and astronomical simulator software (e.g., Starry Night, Stellarium, and the like). Several models have been proposed to interpolate and forecast DT values. Due to the complex behavior of ER, the presented models have significant errors in predicting the future values of DT. Structurally, all mentioned methods have just employed previous DT values for modeling. The weakness of these models is probably the use of the DT parameter alone in the modeling process. In this study, a novel approach was proposed to model and forecast DT values with respect to astronomical-origin-based effective factors in the ER. The remaining parts of the article are organized as follows:

Related works are presented in Section 2. In addition, Section 3 discusses introducing and implementing the proposed method for modeling DT values. The results and discussion are provided in Sections 4 and 5, respectively, and Section 6 presents the conclusion.

2- Related works

As mentioned before, DT values are needed to convert between TT and UT. To this end, researchers must be able to forecast or interpolate DT values. In the recent past, several models have been proposed to interpolate and forecast DT values. Table 1 represents these models along with their structures. As shown in Table 1, most of the models are polynomial-based.

Jean Meeus proposed two 9th/10th order polynomials covering the time span 1800 to 1997 with a Maximum Absolute Errors (MaxAE[1]) of 1.04 s [20] in the second edition of his *Astronomical Algorithms* (1998). Two years later, Jean Meeus and Larry Simons introduced eight 4th order polynomials to cover the period between 1620 and 2000 with a MaxAE of 3.2 s [10]. In *Astronomy on the Personal Computer*, seven 3rd-order polynomials were applied to cover the period between 1825 and 2000 with a MaxAE of 2.16 SI s [21]. Islam, Sadiq, and Shahid-Qureshi (2018), like Meeus and Simons, used eight 4th order polynomials to model DT values. Their work covers the period between 1620 and 2000 with a MaxAE of 0.84 SI s [22]. One year later, Fred Espenak and Jean Meeus used one 2nd-order polynomials in their work with a MaxAE of 6.97 s [23]. The last polynomial-based model was reported in 2014 with nine 4th-order polynomials and MaxAE of 0.6 SI s [24].

Hakimi et.al in 2011 applied a feedforward multilayer perceptron with two hidden layers to model and forecast DT values for the time span 1620 to 2010. This architecture has 29 Artificial Neurons (ANs) for the first hidden layer, 16 for the second hidden layer, and 1 for the output layer. The MaxAE of this model was reported at about 0.55 s [9]. The

1 $MaxAE = \max\left(\left|Target_{(i)} - Output_{(i)}\right|\right)$, where $|.|$ is the absolute operator.

Table 1. The structure of prior models for the interpolation and prediction of DT values

Model	Structure of the Model
[20]	One 9th and one10th-order polynomials
[10]	Eight 4th-order polynomials
[22]	Eight 4th-order polynomials
[23]	One 2th-order polynomials
[9]	MLP with two hidden layers
[21]	Seven 3th-order polynomials
[24]	Nine 4th-order polynomials
[25]	RBTM (N=69 and LR=4)

Note. MLP: Multilayer perception

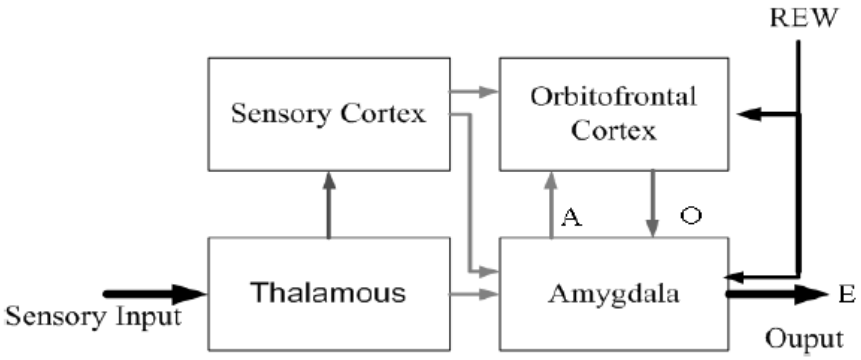

Fig. 2. Components diagram of the amygdala-orbitofrontal subsystem

last method is an RBTM-based model proposed by Hakimi et.al in 2021. RBTM uses a Knowledge Base (KB) to select a proper reward value for each step time. The next value is generated using this reward and the prior DT values. The MaxAE of RBTM is about 0.58 [25].

3- DT modeling based on brain emotional learning

The human brain is a complex system with the ability to simultaneously receive input from the five senses, make decisions, and command different body muscles. In recent years, several efforts have been made to understand how the human brain works with this level of complexity. Accordingly, various computational models have been inspired by the human brain. One of these important models is the amygdala-orbitofrontal subsystem model. The amygdala-orbitofrontal subsystem, which is the main basis of many computational models, has a simple structure. Fig. 2 shows the components of this subsystem. This subsystem consists of four parts interacting to form connections between conditioned and unconditioned stimuli. Besides, it uses a simplified computational method inspired by brain emotional learning. Various architectures of the amygdala-orbitofrontal system have been presented and used in applications such as forecasting (especially forecasting of chaotic time series) [26]–[37].

This paper suggests Memory-Based Brain Emotional Learning (MBBEL) as a novel approach to the amygdala-orbitofrontal system along with specialized memory for amygdala and orbitofrontal parts to model Earth's rotation variations. This model employs the time series of DT values (as the principal input signal) and time series related to solar

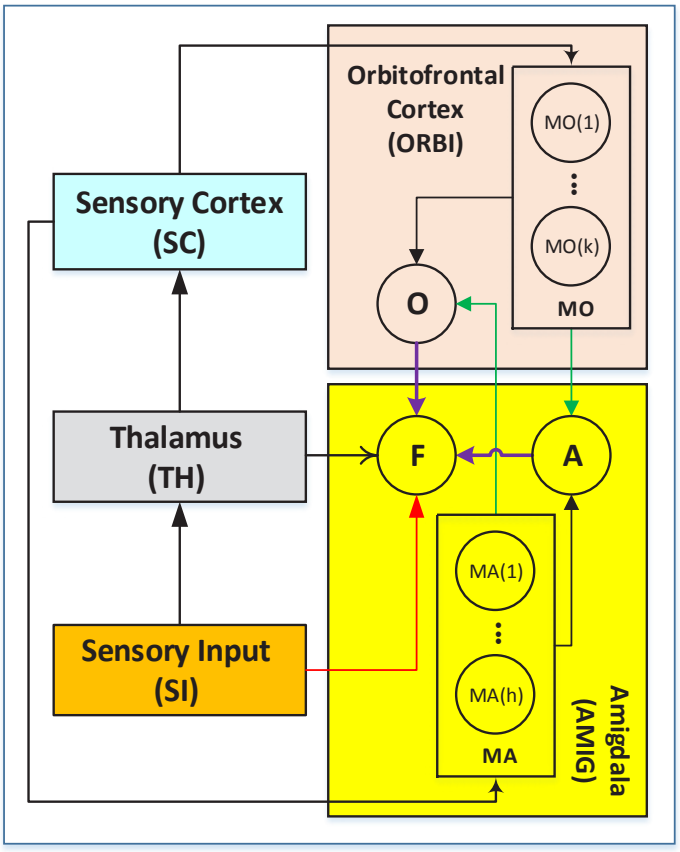

Fig. 3. Architecture diagram of the proposed model (MBBEL)

activities and the gravitational force of the sun, the moon, and solar system planets (as the emotional input signals).

3- 1- Memory-Based Brain Emotional Learning (MBBEL)

Fig. 3 shows the architecture of MBBEL. Based on this figure, MBBEL consists of five main parts: Sensory Input (*SI*), Thalamus (*TH*), Sensory Cortex (*SC*), Amygdala (*AMIG*), and Orbitofrontal cortex (*ORBI*). Table 2 depicts a brief description of parts and their connections in MBBEL. To describe MBBEL's architecture, we used machine-learning terminology instead of neuro-scientific terms.

In MBBEL, *SI* receives principal and emotional input signals (time series) and labels them as shown in Eq. (2). Here, $SI^{p}_{(t)}$ and $SI^{e}_{(t)}$ are related to the principal and emotional input signals, respectively.

$$SI^{S}_{(t)}:\begin{cases} SI^{p}_{(t)} \\ SI^{e^1}_{(t)}\ldots.SI^{e^n}_{(t)} \end{cases} \quad (2)$$

Stationarizing a time series through differencing is an integral part of fitting some forecasting models [38]. *TH* receives the principal and emotional signals from *SI* and converts them to stationary ones (where needed[1]) using Eq. (3). The outputs of *TH* are sent to the *SC*. Besides, *TH* conveys a copy of the principal input to the *AMIG*.

$$TH^{S}_{(t)} = SI^{S}_{(t)} - SI^{S}_{(t-1)} \quad (3)$$

SC generates input-target pairs of training and testing data based on Eq. (4) and Eq. (5) and conveys $SC^{p}_{(t)}$ and $SC^{e}_{(t)}$ to *ORBI* and *AMIG,* respectively.

$$SC^{p}_{(t)} = \begin{Bmatrix} Inputs : [TH^{p}_{(t-k)} TH^{p}_{(t-k-1)}.\ldots TH^{p}_{(t-1)}] \\ Output : TH^{p}_{(t)} \end{Bmatrix} \quad (4)$$

1 - Augmented Dickey-Fuller test is a useful statistical test to determine a time series is stationary or non-stationary.

$$SC^{e}_{(t)} = \begin{Bmatrix} Inputs : [TH^{p}_{(t-s)} TH^{p}_{(t-s-1)} \dots . TH^{p}_{(t-1)} \\ TH^{e^{(j)}}_{(t-h)} TH^{e^{(j)}}_{(t-h-1)} \dots . TH^{e^{(j)}}_{(t-1)}] \\ \\ Output : \ TH^{i}_{(t)} \end{Bmatrix} \quad (5)$$

where TH^{p} and $TH^{e^{(j)}}$ are related to the principal signal and j[th] emotional signal, respectively.

ORBI is divided into two subparts: MO (Memory related to the *ORBI*) and O (Output of the *ORBI*). On the other hand, *AMIG* has three subparts: MA (Memory related to the *AMIG*), A (Output of *AMIG*), and F (Fusion of the outputs of A and O as the output of the MBBEL).

MO consists of several memory units ($MO^{(1)}$ to $MO^{(k)}$) receiving input-target pairs with different lengths from the **CS**. Each memory unit has more than one MultiLayer Perceptron (MLP) model combined based on boosting method (Eq. 6). Boosting is a general method for improving the performance of learning algorithms and tends to be robust to overfitting [39], [40]. The outputs of memory units are sent to the O. Afterward, these outputs are combined using Eq. (7) and are conveyed to A as the *ORBI* feedback.

Like MO, MA has several memory units with different input-target pairs from the MO. These units are modeled by Eq. (8), and their outputs are sent to the A. These outputs are combined using Eq. (9) and sent to the O as the *AMIG* feedback.

The number of MLP models and their architecture can differ in MO and MA units. After the training stage, MO and MA play the role of LongTerm and ShortTerm memories of *ORBI* and *AMIG,* respectively. On the other hand, based on different input-target pairs related to the principal and emotional input signals, MO and MA can be considered as the logical and emotional memory of MBBEL, respectively.

$$MOM^{(i)}_{(t)} = \text{Boosting method} \begin{cases} The\ number\ of\ \ MLP\ models : X \\ \ \ Input - Target\ pairs : SC^{p}_{(t)} \end{cases} \quad (6)$$

$$MO_{(t)} = \sum_{i=1}^{k} MOM^{(i)}_{(t)} / k \quad (7)$$

$$MAM^{(j)}_{(t)} = \text{Boosting method} \begin{cases} The\ number\ of\ \ MLP\ models : Y \\ \ \ Input - Target\ pairs : SC^{e}_{(t)} \end{cases} \quad (8)$$

$$MA_{(t)} = \sum_{j=1}^{h} MAM^{(j)}_{(t)} / h \quad (9)$$

O and A receives inputs from memory units and calculate the output of *ORBI* and *AMIG* using Eq. (10) and Eq. (11), respectively.

$$O_{(t)} = \left(MA_{(t)} + \sum_{i=1}^{k} MOM^{(i)}_{(t)} \right) / \left(k + 1 \right) \quad (10)$$

$$A_{(t)} = \left(O_{(t)} + \sum_{j=1}^{h} MAM^{(j)}_{(t)} \right) / \left(h + 1 \right) \quad (11)$$

In node F, the outputs of A and O are fused and then converted to the principal input domain using Eq. (12) and Eq. (13), respectively.

$$FM_{(t)} = \text{Boosting method} \begin{cases} The\ number\ of\ \ MLP\ models : Z \\ \ \ Inputs : O_{(t)}\ and\ A_{(t)} \\ Target : TH^{1}_{(t)} \end{cases} \quad (12)$$

$$F_{(t)} = FM_{(t)} + SI^{1}_{(t-1)} \quad (13)$$

3- 2- Used Data

3- 2- 1- DT Values

In this study, we use time series of DT from 1900 to 2018 with a yearly time interval. The values are accessible each year in the Astronomical Almanac (pp. K8-K9), published annually by the Nautical Almanac Offices of the US Naval Observatory (Washington DC) and the Rutherford Appleton Laboratory (Cambridge) [9]. Fig. 1 shows DT values from 1620 to 2018.

3- 2- 2- Solar Activities

The sun is a magnetic variable star that fluctuates on different time scales. The changes in the Sun cause effects in space, in the atmosphere, and on the Earth's surface [6]-[8]. Sunspots are dark regions that appear on the surface of the sun. Sunspots during the time reflect the intensity and weakness of solar activity [41]. The time series of the yearly mean Sunspot Number (SSN) can be obtained from **http://sidc.oma.be/silso/datafiles**. This time series is used for modeling and forecasting solar cycles and evaluating different forecasting models [42]. Fig. 4 shows the values of SSN from 1900 to 2018 used in this study.

Table 2. A brief description of the role and interaction of the components of the EMBBEL model

Main Part	Subparts	Role	Inputs	Output	Equation Number
Sensory Input (SC)	---	Getting of the principal and emotional signals	DT, SSN and MF	$SI^{S}_{(t)}$	Eq. (2)
Thalamus (TH)	---	Conversion of signals to stationary ones	$SI^{S}_{(t)}$ and $SI^{S}_{(t-1)}$	$TH^{S}_{(t)}$	Eq. (3)
Sensory Cortex (SC)	---	Generation and distribution of input-target pairs	$TH^{S}_{(t)}$	$SC^{p}_{(t)}$	Eq. (4)
				$SC^{e}_{(t)}$	Eq. (5)
Orbitofrontal Cortex (ORBI)	MO(i)	i[th] unit of principal memory	$SC^{p}_{(t)}$	$MOM^{(i)}_{(t)}$	Eq. (6)
	MO	Memory related to ORBI	$MOM^{(1)}_{(t)}$ to $MOM^{(k)}_{(t)}$	$MO_{(t)}$	Eq. (7)
	O	Generation of output of the ORBI	$MOM^{(1)}_{(t)}$ to $MOM^{(k)}_{(t)}$ and $MA_{(t)}$	$O_{(t)}$	Eq. (10)
Amygdala (AMIG)	MA(j)	j[th] unit of emotional memory	$SC^{e}_{(t)}$	$MAM^{(j)}_{(t)}$	Eq. (8)
	MA	Memory related to AMIG	$MAM^{(1)}_{(t)}$ to $MAM^{(h)}_{(t)}$	$MA_{(t)}$	Eq. (9)
	A	Output of the AMIG	$MAM^{(1)}_{(t)}$ to $MAM^{(h)}_{(t)}$ and $MO_{(t)}$	$A_{(t)}$	Eq. (11)
	F	Fusion of the AMIG and ORBI outputs	$TH^{1}_{(t)}$, $O_{(t)}$ and $A_{(t)}$	$FM_{(t)}$	Eq. (12)
			$SI^{p}_{(t-1)}$ and $Out_{(t)}$	$F_{(t)}$	Eq. (13)

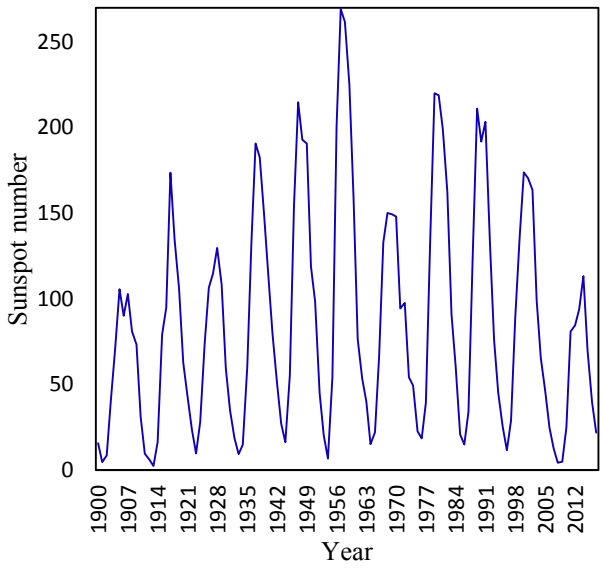

Fig. 4. Time series diagram of yearly mean sunspot number from 1900 to 2018

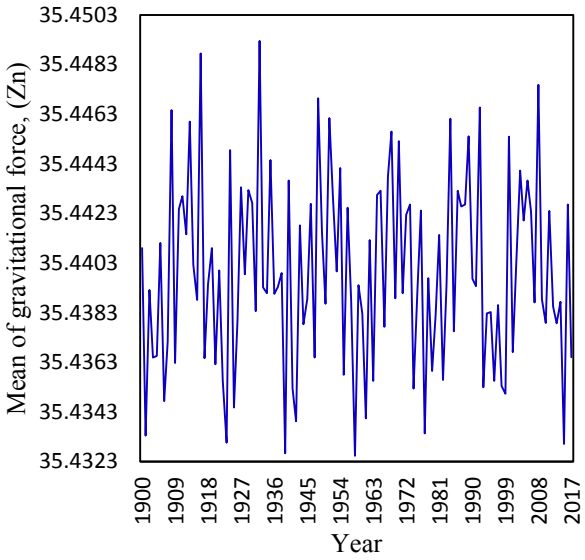

Fig. 5. Time series diagram of yearly mean of the total gravitational force (MF) from 1900 to 2018

3- 2- 3- Gravitational force of the sun, the moon, and solar system planets on the Earth

Every planetary body (including the Earth) is surrounded by its own gravitational field. This field can be conceptualized by Newtonian physics as exerting an attractive force on all objects. The most known effects of the Gravitational Force (GF) of solar system objects on ER are the Earth tides, precession, and nutation [43], [44]. The effect of the gravitational force is related to the distance of the center of these objects from the center of the Earth and the mass of each of them. Besides, the total gravitational force to the Earth is related to their position in space [45].

In this study, we calculated the time series of yearly mean GF values from 1900 to 2018. At first, the mass, distance, and position of the Sun, Moon, Mercury, Venus, Mars, Jupiter, Saturn, Uranus, and Neptune were obtained relative to the center of the Earth using Starry Night 6 Pro Plus software. Next, their gravitational force was calculated using Newton's law of universal gravitation formula. Finally, the yearly mean of the total gravitational force was computed and named MF. It is of note that the MF scale is Zettanewton[1] (*Zn*). Fig. 5 represents this time series.

3- 3- Implementation of MBBEL

We implemented MBBEL using IBM SPSS Modeler 18.0 software. The values of variables from 1900 to 2018 were divided into two parts: 1) The data from 1900 to 2000 were selected for the training stage. 2) The residuals (2000 to 2018) were applied to evaluate the accuracy of forecasting DT values by MBBEL.

1 **Zetta** is a decimal unit prefix in the metric system denoting a factor of 10^{21} or 1,000,000,000,000,000,000,000. The prefix, denoted by the symbol **Z**, was added as an SI prefix to the International System of Units (SI) in 1991.

In implemented MBBEL, SI gets DT (as the principal input signal), SSN, and MF (as emotional input signals). Eq. (14) shows labels of SI. Table 3 depicts the used input-target pairs of memory units and fusion parts along with the structure of the boosting method.

$$SI_{(t)}^{S}:\begin{cases} SI_{(t)}^{p}=DT_{(t)} \\ SI_{(t)}^{e^1}=SSN_{(t)} \\ SI_{(t)}^{e^2}=MF_{(t)} \end{cases} \tag{14}$$

Used models in MO, MA, and F must be trained offline separately. At first, memory units of MO and MA were trained. Then, the model related to the F was trained using the outputs of A and O.

4- Results

4- 1- MBBEL results

The MBBEL was implemented, and its output results were determined accordingly. The mean absolute error (MAE) and MaxAE of the training stage were 0.011 and 0.051, respectively. Further, MAE and MaxAE in the test stages were 0.1 and 0.295, respectively.

The proposed model consisted of AMIG, ORBI, and F parts, which are responsible for memorizing and making decisions against new input signals. The AMIG and ORBI parts make emotional and logical decisions, respectively. AMIG and ORBI outputs are received as input, and the final output of MBBEL is produced in the F part. Therefore, checking the accuracy of the operation of each of these three sections allows for identifying which part performs better. Furthermore, it can be inferred whether the fusion of

Table 3. Structure of input-target vectors and boosting method used in different components of MBBEL

	Label	Inputs	Target	Structure of Boosting method
Memory units related to ORBI	$SC_{(t)}^{1}$	$DT_{(i)}$ & $DT_{(i-1)}$ & $DT_{(i-2)}$	$DT_{(i+1)}$	Base Models: MLP Hidden Layers: [15, 5] The number of base models: 150 Combining rule: Mean
	$SC_{(t)}^{2}$	$DT_{(i)}$ & $DT_{(i-1)}$ & $DT_{(i-2)}$ & $DT_{(i-3)}$	$DT_{(i+1)}$	
	$SC_{(t)}^{3}$	$DT_{(i)}$ & $DT_{(i-1)}$ & $DT_{(i-2)}$ & $DT_{(i-3)}$ & $DT_{(i-4)}$	$DT_{(i+1)}$	
Memory units related to AMIG	$SC_{(t)}^{4}$	$DT_{(i)}$ & $DT_{(i-1)}$ & $DT_{(i-2)}$ & $MF_{(i-3)}$ & $SSN_{(i-4)}$	$DT_{(i+1)}$	
	$SC_{(t)}^{5}$	$DT_{(i)}$ & $DT_{(i-1)}$ & $DT_{(i-2)}$ & $SSN_{(i-3)}$ & $SSN_{(i-4)}$	$DT_{(i+1)}$	
	$SC_{(t)}^{6}$	$DT_{(i)}$ & $DT_{(i-1)}$ & $DT_{(i-2)}$ & $MF_{(i)}$ & $MF_{(i-1)}$	$DT_{(i+1)}$	
	$SC_{(t)}^{7}$	$DT_{(i)}$ & $DT_{(i-1)}$ & $DT_{(i-2)}$ & $MF_{(i-3)}$ & $SSN_{(i-3)}$	$DT_{(i+1)}$	
Fusion model	$FM_{(t)}$	$O_{(t)}$ & $A_{(t)}$	$DT_{(i+1)}$	

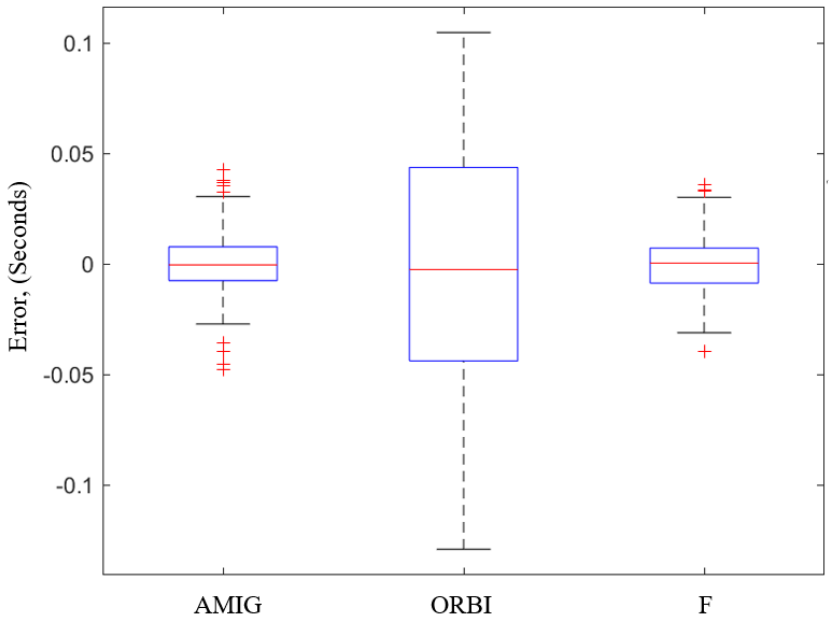

Fig. 6. Box chart of errors of the main parts of MBBEL

the results in F is effective. To review this issue, the results were checked more closely by calculating the error of each main part of MBBEL in the form of a box chart (Fig. 6). Based on data in Fig. 6, the F, AMIG, and ORBI parts perform better, respectively. Table 4 provides the accuracy of memory units and the fusion part of MBBEL and reports the order of effective input elements in the modeling process. The importance value of each input element is stated just below the name of the corresponding element. Here, a larger number means more importance of the element in the input vector. According to Table 4, F, memory units of AMIG, and memory units of ORBI perform better, respectively. Thus, it can be claimed that the fusion of results in F is effective, and the overall performance is better than that of AMIG and ORBI, separately.

4- 2- MBBEL results against prior models

To evaluate the results of MBBEL, the error of the training and testing stages was compared with that of previous models. Table 5 presents this comparison. Moreover, Fig. 7 compares the errors of the forecasted DT values from 2000 to 2018 using all the models. Based on data in Table 5 and Fig.

Table 4. Accuracy of memory units and fusion part of the MBBEL predictor, along with importance values of each variable in the modeling process

MBBEL Parts		The order of effective variables in the modeling process					Accuracy in percent
		First PIV*	Second PIV*	Third PIV*	Forth PIV*	Fifth PIV*	
ORBI	MO(1)	$DT_{(i-1)}$ 0.3679	$DT_{(i-2)}$ 0.3397	$DT_{(i)}$ 0.2923	---	---	97.0
	MO(2)	$DT_{(i-1)}$ 0.2790	$DT_{(i-2)}$ 0.2725	$DT_{(i)}$ 0.2317	$DT_{(i-3)}$ 0.2168	---	98.2
	MO(3)	$DT_{(i-1)}$ 0.2432	$DT_{(i-2)}$ 0.2340	$DT_{(i)}$ 0.2109	$DT_{(i-3)}$ 0.1889	$DT_{(i-4)}$ 0.1229	98.7
AMIG	MA(1)	$DT_{(i-1)}$ 0.3555	$DT_{(i-2)}$ 0.3336	$DT_{(i)}$ 0.3074	$MF_{(i-3)}$ 0.0031	$SSN_{(i-3)}$ 0.0004	99.7
	MA(2)	$DT_{(i-1)}$ 0.3640	$DT_{(i-2)}$ 0.3292	$DT_{(i)}$ 0.3050	$MF_{(i)}$ 0.0011	$MF_{(i-1)}$ 0.0007	99.5
	MA(3)	$DT_{(i-1)}$ 0.3600	$DT_{(i-2)}$ 0.3378	$DT_{(i)}$ 0.3015	$SSN_{(i-3)}$ 0.0007	$SSN_{(i-4)}$ 0.00008	99.7
	MA(4)	$DT_{(i-1)}$ 0.3476	$DT_{(i-2)}$ 0.3368	$DT_{(i)}$ 0.3101	$MF_{(i-3)}$ 0.0052	$SSN_{(i-4)}$ 0.0003	99.7
F		AMIG 0.5553	ORBI 0.4447	---	---	---	99.9

Note. *PIV: Predictor importance value in the modeling process

7, errors in the train and test stages of MBBEL significantly decreased compared to the results of previous models.

5- Discussion

Table 5 and Figure 7 show that the error of the MBBEL in modeling and forecasting DT values has been significantly reduced compared to all previously presented methods. Although previous methods were successful in modeling, their forecasting error increased exponentially over time. The models [10, 20-24] are structurally different in terms of order and number of polynomial equations. Based on the data in Table 5, they are mainly suitable for interpolation. Model [9] uses a two-layer artificial neural network structure, and this structure allows this model to forecast the future values of DT. However, due to the complex nature of the problem, the forecasting error of this method is also high. The overfitting problem may be a reason for this decrease in generalization. In any case, the last presented method used the RBTM architecture, which was employed for complex system modeling [25]. RBTM applies no learning algorithm and the number of its parameters is slight. Due to the use of its own rule-base, RBTM has provided an extremely lower forecasting error than other previous methods.

The examination of the structure and error of previous models revealed that better results have been obtained with the methods with the ability to model complex systems. However, these methods only utilized DT values to model the complex behavior of ER. In this research, the data of factors affecting the ER (SSN and MF), along with its descriptive factor of ER (DT), was first used for modeling and forecasting by the MBBEL method. MBBEL is a new architecture based on the amygdala-orbitofrontal subsystem with a completely different inference method. It introduces logical and emotional memory units with different input vector lengths (e.g., short-term and medium-term). Additionally, it applies the boosting method to reduce bias, as well as the variance of memory units and the fusion of logical and emotional decision-making units. Based on Fig. 7, MBBEL could control the final output and keep the forecasting errors close to zero by using emotional and logical parts and their fusion. The findings of this research demonstrated that using auxiliary variables (SSN and MF), along with the main variable (DT) can increase the accuracy

Table 5. Comparison between the MBBEL's error and previous models in the training and testing stages

Model	Train/Modeling			Test/forecasting		
	Duration of modeling	MAE (Seconds)	MaxAE (Seconds)	Duration of Forecasting	MAE (Seconds)	MaxAE (Seconds)
[20]	1800 - 1998	0.40	1.04	2000-2018	236.78	841.09
[10]	1620 - 2000	0.87	3.20	2000-2018	17.97	58.49
[22]	1620 - 2000	0.25	0.84	2000-2018	18.39	60.76
[23]	1986 - 2010	2.17	6.97	2000-2018	6.33	11.05
[9]	1620 - 2011	0.11	0.55	2011-2018	18.10	40.89
[21]	1825 - 2000	0.23	2.16	2000-2018	20.28	47.52
[24]	1620 - 2014	0.21	0.60	2014-2018	2.00	3.92
[25]	1800 - 2000	0.17	0.58	2000-2018	1.04	1.40
MBBEL	1900 - 2000	**0.01**	**0.01**	2000-2018	**0.10**	**0.29**

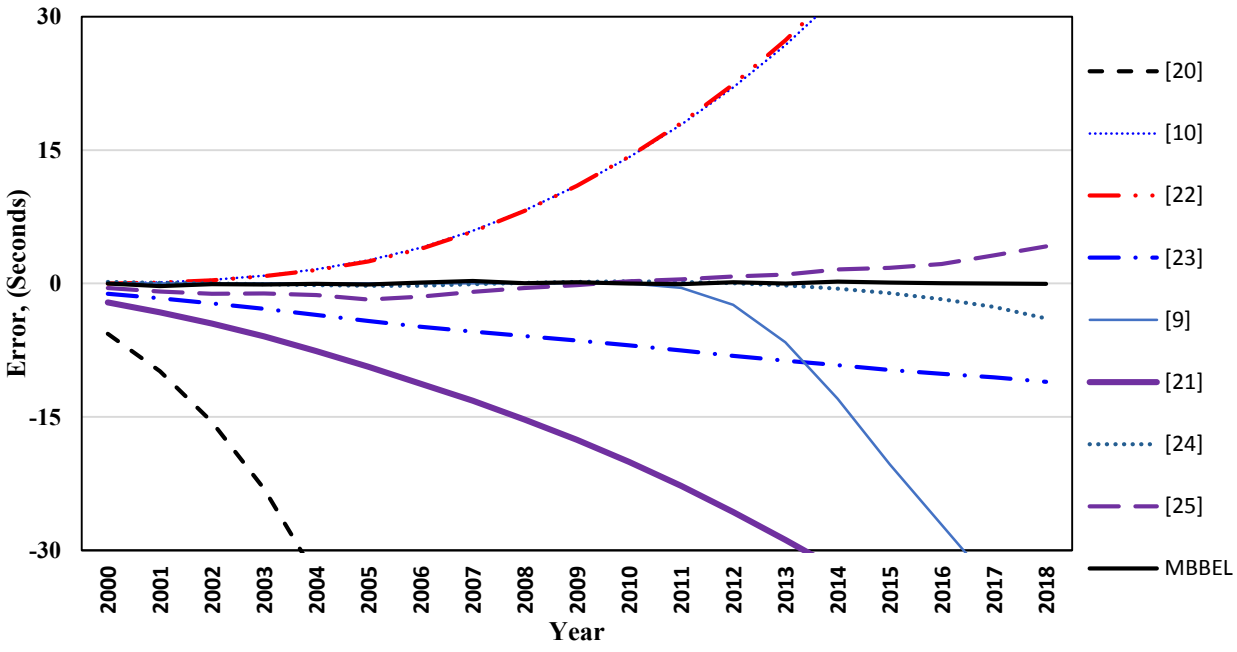

Fig. 7. Error diagram of the forecasted DT values from 2000 to 2018 using MBBEL and prior models

of modeling the main variable.

Limited access to the data of other factors affecting ER has made it difficult to model and forecast DT values. Future studies can obtain and use the data of these factors and can apply the other methods of modeling complex systems.

6- Conclusion

This paper introduced MBBEL as a novel approach to the amygdala-orbitofrontal system along with specific memory for amygdala and orbitofrontal parts for modeling DT values (as the principal input signal) with respect to SSN and MF (as the emotional input signals). SSN and MF are two known astronomical-origin-based effective factors on the Earth's rotation. In the modeling process, the data from 1900 to 2000 and 2000 to 2018 were used for training and testing, respectively. For evaluation of MBBEL, their results were compared against those of eight prior models. As shown in Table 5 and Fig. 7, the MBBEL results considerably improved compared to the previous models. This research showed that using auxiliary variables along with the main variable can enhance the accuracy of modeling the main variable.

References

[1] C. Audoin, B. Guinot, and others, "The measurement of time," Time, Freq. At. Clock, New York, 2001.

[2] J. O. Dickey, "Earth rotation variations from hours to centuries," Highlights Astron., vol. 10, pp. 17–44, 1995.

[3] W. Schlüter, A. Böer, R. Dassing, H. Hase, P. Sperber, and R. Kilger, "TIGO-Transportable Integrated Geodetic Observatory, status of the project," Proc. Dyn. Solid Earth, Pasadena, 1995.

[4] R. A. Del Rio, "The influence of global warming in Earth rotation speed," in Annales Geophysicae, 1999, vol. 17, no. 6, pp. 806–811.

[5] R. A. Del Rio, D. Gambis, and D. A. Salstein, "Interannual signals in length of day and atmospheric angular momentum," in Annales Geophysicae, 2000, vol. 18, no. 3, pp. 347–364.

[6] R. Del Rio, D. Gambis, D. Salstein, P. Nelson, and A. Dai, "Solar activity and earth rotation variability," J. Geodyn., vol. 36, pp. 423–443, 2003.

[7] R. G. Currie, "Detection of the 11-yr sunspot cycle signal in Earth rotation," Geophys. J. Int., vol. 61, no. 1, pp. 131–140, 1980.

[8] H. Spencer Jones, "The rotation of the earth, and the secular accelerations of the sun, moon and planets," Mon. Not. R. Astron. Soc., vol. 99, p. 541, 1939.

[9] A. R. Hakimi and S. Setayeshi, "A novel approach to delta-T from 1620 to 2010," Mon. Not. R. Astron. Soc., vol. 417, no. 4, pp. 2714–2720, 2011, doi: 10.1111/j.1365-2966.2011.19435.x.

[10] J. Meeus and L. Simons, "Polynomial approximations to Delta T, 1620 (2000 AD," J. Br. Astron. Assoc., vol. 110, 2000.

[11] F.-R. Stephenson and L. V Morrison, "Long-term changes in the rotation of the Earth: 700 BC to AD 1980," Phil. Trans. R. Soc. Lond. A, vol. 313, no. 1524, pp. 47–70, 1984.

[12] J. M. Steele, "Predictions of eclipse times recorded in Chinese history," J. Hist. Astron., vol. 29, no. 3, pp. 275–285, 1998.

[13] F.-R. Stephenson, "Book Review: Historical eclipses and Earth's rotation/Cambridge U Press, 1997," J. Br. Astron. Assoc., vol. 107, p. 220, 1997.

[14] F.-R. Stephenson and J. T. Baylis, "Early Chinese observations of occultations of planets by the Moon," J. Hist. Astron., vol. 43, no. 4, pp. 455–477, 2012.

[15] F.-R. Stephenson and L. J. Fatoohi, "Accuracy of solar eclipse observations made by Jesuit astronomers in China," J. Hist. Astron., vol. 26, no. 3, pp. 227–236, 1995.

[16] F.-R. Stephenson and L. J. Fatoohi, "The Babylonian unit of time," J. Hist. Astron., vol. 25, no. 2, pp. 99–110, 1994.

[17] F.-R. Stephenson and M. A. Houlden, Atlas of Historical Eclipse Maps: East Asia 1500 BC-AD 1900. Cambridge University Press, 1986.

[18] D. F. Crouse, "An Overview of Major Terrestrial, Celestial, and Temporal Coordinate Systems for Target Tracking," 2016.

[19] D. Gambis and B. Luzum, "Earth rotation monitoring, UT1 determination and prediction," Metrologia, vol. 48, no. 4, p. S165, 2011.

[20] J. Meeus, "The effect of Delta T on astronomical calculations," J. Br. Astron. Assoc., vol. 108, pp. 154–156, 1998.

[21] O. Montenbruck and T. Pfleger, Astronomy on the personal computer. Springer, 2013.

[22] S. Islam, M. Sadiq, and M. S. Qureshi, "ASSESSING POLYNOMIAL APPROXIMATION FOR ΔT," J. Basic Appl. Sci., vol. 4, no. 1, pp. 1–4, 2008.

[23] F. Espenak and J. Meeus, "Five Millennium Catalog of Solar Eclipses:-1999 to+ 3000 (2000 BCE to 3000 CE)-Revised," 2009.

[24] M. Khalid, M. Sultana, and F. Zaidi, "Delta: Polynomial Approximation of Time Period 1620--2013," J. Astrophys., vol. 2014, 2014.

[25] A. Hakimi, S. A. Monadjemi, and S. Setayeshi, "An introduction of a reward-based time-series forecasting model and its application in predicting the dynamic and complicated behavior of the Earth rotation (Delta-T values)[Formula presented]," Appl. Soft Comput., vol. 113, 2021, doi: 10.1016/j.asoc.2021.107920.

[26] A. M. Yazdani, A. Mahmoudi, M. A. Movahed, P. Ghanooni, S. Mahmoudzadeh, and S. Buyamin, "Intelligent Speed Control of Hybrid Stepper Motor Considering Model Uncertainty Using Brain Emotional Learning," Can. J. Electr. Comput. Eng., vol. 41, no. 2, pp. 95–104, 2018.

[27] M. Roshanaei, E. Vahedi, and C. Lucas, "Adaptive antenna applications by brain emotional learning based on intelligent controller," IET microwaves, antennas Propag., vol. 4, no. 12, pp. 2247–2255, 2010.

[28] W. Fang, F. Chao, C.-M. Lin, L. Yang, C. Shang, and C. Zhou, "An Improved Fuzzy Brain Emotional Learning Model Network Controller for Humanoid Robots," Front. Neurorobot., 2019.

[29] S. H. Fakhrmoosavy, S. Setayeshi, and A. Sharifi, "A modified brain emotional learning model for earthquake magnitude and fear prediction," Eng. Comput., vol. 34, no. 2, pp. 261–276, 2018.

[30] E. Lotfi, O. Khazaei, and F. Khazaei, "Competitive brain emotional learning," Neural Process. Lett., vol. 47, no. 2, pp. 745–764, 2018.

[31] Q. Wu et al., "Self-Organizing Brain Emotional Learning Controller Network for Intelligent Control System of Mobile Robots," IEEE Access, vol. 6, pp. 59096–59108, 2018.

[32] S. Motamed, S. Setayeshi, and A. Rabiee, "Speech emotion recognition based on brain and mind emotional learning model," J. Integr. Neurosci., no. Preprint, pp. 1–15, 2018.

[33] M. Moradi Zirkohi, "An Efficient Optimal Fractional Emotional Intelligent Controller for an AVR System in Power Systems," J. AI Data Min., vol. 7, no. 1, pp. 191–200, 2019.

[34] R. Ayanzadeh, A. S. Z. Mousavi, and S. Setayeshi, "Fossil fuel consumption prediction using emotional learning in Amygdala," in 2011 19th Iranian Conference on Electrical Engineering, 2011, pp. 1–6.

[35] Z. Farhoudi, S. Setayeshi, and A. Rabiee, "Using learning automata in brain emotional learning for speech emotion recognition," Int. J. Speech Technol., vol. 20, no. 3, pp. 553–562, 2017.

[36] S. H. Fakhrmoosavy, S. Setayeshi, and A. Sharifi, "An intelligent method for generating artificial earthquake records based on hybrid PSO--parallel brain emotional learning inspired model," Eng. Comput., vol. 34, no. 3, pp. 449–463, 2018.

[37] J. Zhao, C.-M. Lin, and F. Chao, "Wavelet Fuzzy Brain Emotional Learning Control System Design for MIMO Uncertain Nonlinear Systems," Front. Neurosci., vol. 12, 2018.

[38] R. Adhikari and R. K. Agrawal, "An introductory study on time series modeling and forecasting," arXiv Prepr. arXiv1302.6613, 2013.

[39] H. Schwenk and Y. Bengio, "Boosting neural networks," Neural Comput., vol. 12, no. 8, pp. 1869–1887, 2000.

[40] R. Meir and G. Rätsch, "An introduction to boosting and leveraging," in Advanced lectures on machine learning, Springer, 2003, pp. 118–183.

[41] M. G. Orozco-Del-Castillo, J. C. Ortiz-Alemán, C. Couder-Castañeda, J. J. Hernández-Gómez, and A. Solís-Santomé, High solar activity predictions through an artificial neural network, vol. 28, no. 6. 2017. doi: 10.1142/S0129183117500759.

[42] H. Iijima, H. Hotta, S. Imada, K. Kusano, and D. Shiota, "Improvement of solar-cycle prediction: Plateau of solar axial dipole moment," Astron. Astrophys., vol. 607, p. L2, 2017.

[43] G. A. Krasinskii, E. I. Saramonova, M. L. Sveshnikov, and E. S. Sveshnikova, "Universal time, lunar tidal deceleration and relativistic effects from observations of transits, eclipses and occultations in the XYIII-XX centuries," Astron. Astrophys., vol. 145, pp. 90–96, 1985.

[44] M.-F. Loutre, "Earth history: Sediments to planetary motion," Nature, vol. 409, no. 6823, p. 991, 2001.

[45] S. Chandrasekhar, Newton's Principia for the common reader. Oxford University Press, 2003.

HOW TO CITE THIS ARTICLE

A. Hakimi, S. A. Monadjemi, S. Setayeshi, Modeling of the Earth's rotation variations using a novel approach inspired by the brain emotional learning, AUT J. Model. Simul., 54(2) (2022) 173-184.

DOI: 10.22060/miscj.2023.21110.5271